Hindawi
Advances in Meteorology
Volume 2019, Article ID 7529263, 16 pages
https://doi.org/10.1155/2019/7529263

Research Article

Numerical Analysis on the Effects of Binary Interaction between Typhoons Tembin and Bolaven in 2012

Zhipeng Xian and Keyi Chen

School of Atmospheric Sciences, Chengdu University of Information Technology, 610225 Chengdu, China

Correspondence should be addressed to Keyi Chen; ckydlt@aliyun.com

Received 7 November 2018; Revised 14 February 2019; Accepted 26 February 2019; Published 3 April 2019

Academic Editor: Mario M. Miglietta

The binary interaction is one of the most challenging factors to improve the forecast accuracy of multiple tropical cyclones (TCs) in close vicinity. The effect of binary interaction usually results in anomalous track and variable intensity of TCs. A typical interaction type, one-way influence mode, has been investigated by many studies which mainly focused on the anomalous track and record-breaking precipitation, such as typhoons Morakot and Goni. In this paper, a typical case of this type, typhoons Tembin and Bolaven, occurred in the western North Pacific in August 2012, was selected to study how one typhoon impacts the track and intensity of the other one. The vortex of Tembin or Bolaven and the monsoon circulation were removed by a TC bogus scheme and a low-pass Lanczos filter, respectively, to carry out the numerical experiments. The results show that the presence of monsoon made the binary interaction more complex by affecting the tracks and the translation speeds of the TCs. The influence of Bolaven on the track of Tembin was more significant than the influence of Tembin on the track of Bolaven, and the looping track of Tembin was also affected by the external surrounding circulation associated with Bolaven. The absence of Tembin was not conducive to the development of Bolaven due to stronger vertical wind shear condition and the less kinetic energy being transported to upper troposphere. Note that the above analysis demonstrates the interacting processes between TCs and sheds some light on the prediction of binary TCs.

1. Introduction

The anomalous track and intensity of tropical cyclone (TC) caused by binary typhoon effect is an important topic in atmospheric sciences. In the early 1920s, Fujiwhara [1] found that two vortices would interact each other when they are close to each other. Brand [2], who analyzed the relationship between angular change and separation distance for 22 pairs of binary typhoons in the western North Pacific, suggested that the binary typhoon effect was related to the scale and intensity of typhoons and further indicated that two typhoons start to rotate when the separation distance is less than 750 miles. Lander and Holland [3] used a reference frame with unweighted approximation to centroid to make a detailed analysis of the behaviour of multiple-vortex interactions in the western North Pacific. They presented a common model of binary interaction that contains the major elements of approach, sudden capture, and then a period of steady cyclonic orbit, followed by a sudden escape or a merger. It further indicated that the vortices would be captured when the separation distance is less than 600 miles. Since many cases of binary typhoons whose tracks are quite different from the mutual advection (Fujiwhara type), Carr et al. [4] and Carr and Elsberry [5] categorized binary typhoon interaction processes and proposed four conceptual models: the direct interaction conceptual model, which includes one-way influence, mutual interaction, and merge modes; the semidirect interaction conceptual model; the indirect interaction conceptual model; and binary cyclone contribution to reverse-oriented trough formation (a monsoon trough with a southwest-northeast orientation, which will occur when two or more TCs locating along a zonally oriented monsoonal cloud band move relative to one another [6]). However, due to the lack of observations, it is difficult to explain how the binary typhoon effect works between the TCs. For this reason, the numerical simulation is considered one of the available methods to investigate it.

Xu et al. [7] studied a binary typhoons case, Morakot and Goni, which occurred in 2009. They pointed out that the existence of Goni played an important role in maintaining the intensity of Morakot, resulting in the heavy rainfall increasing over Taiwan, as compared to the experiment removing Goni's circulation. But, Wu et al. [8] drew an opposite conclusion for the same binary typhoons case. They carried out a set of experiments with modifying the intensity of Morakot in its initial conditions to evaluate the factors affecting the interaction between the two TCs. The results showed that Morakot had a greater impact on the motion and was conducive to intensifying the strength of Goni, whereas Goni, located upstream of the southwesterly flow, intercepted part of the water vapor being transported to Morakot, making Morakot weaken. Xu et al. [9] applied the same experiment design to study another binary typhoons case, Bopha and Saomai, which occurred in 2006. They indicated that Saomai's track and intensity responded to the change in the intensity of Bopha and Bopha had opposite effects at different development stages of Saomai.

The interaction between typhoons Tembin and Bolaven resulted in strong winds and heavy rain in both Taiwan and Fujian provinces of China in August 2012. Reviewing the evolution of Tembin and Bolaven (Figure 1(a)) shows that the former was characterized by a looping track and slow translation speeds, while the latter was characterized by northwestward motion. It is interesting that the tracks of Tembin and Bolaven are quite similar to Morakot and Goni's, especially the looping tracks of Tembin and Goni. According to the studies of Carr et al., the two pairs of binary typhoons can be both considered as the one-way influence of the direct interaction mode in which the track of a smaller TC that is embedded in the circulation of a larger TC has an orbiting motion but causes no significant track alteration of the larger TC due to its much smaller circulation. In other words, the track of a smaller TC (i.e., Tembin and Goni) that is dominated by a larger TC (i.e., Bolaven and Morakot) has a cyclonic looping motion. Previous studies [10, 11] on Tembin and Bolaven mainly focused on the complicated tracks, but these were insufficient for the investigation of the two typhoons' intensities. As mentioned above, for the one-way influence of interaction mode, such as Morakot and Goni, the answer to the question of how the binary typhoon effect affects the track and intensity of TCs remains unclear. Therefore, it is worthy carrying out a study on this interaction mode to investigate how one typhoon impacts the track and intensity of another one.

2. Data and Methods

2.1. Data. The data used as the initial and boundary conditions in this study are the final (FNL) global analysis data (resolution: $1^\circ \times 1^\circ$) from the National Center for Environmental Prediction/National Center for Atmospheric Research (NCEP/NCAR) with the time resolution of 6 hours and the real-time global analysis sea surface temperature (SST) dataset (RTG_SST, $0.5^\circ \times 0.5^\circ$) from the National Center for Environmental Prediction/National Oceanic and Atmospheric Administration (NCEP/NOAA) with the time resolution of 24 hours. The best track of the TCs is obtained from the International Best Track Archive for Climate Stewardship (IBTrACS) [12] with the 6-hour time resolution, which contains the information about the central location of the TCs, the minimum pressure, the maximum wind near the TCs' center, the maximum wind radius, etc.

2.2. TC Bogus Scheme. TC bogus is a TC initial processing scheme of Fredrick et al., and the method description partly reproduces their wording [13]. The scheme can either introduce a new vortex or remove an existing one. The vortex removal is done as follows. Firstly, use the best track location of the TC and 400 km as the search radius to look for the maximum relative vorticity in the pressure field nearest the surface. The grid point where the maximum relative vorticity is located serves as the center of the vortex to be removed. The vorticity and divergence outside the radius of 300 km of the vortex's center are set to zero by the scheme. Then, use the successive overrelaxation method to solve the following equations for the stream function, velocity potential, nondivergent wind, and divergent wind:

$$\begin{aligned} \nabla^2 \psi &= \zeta, \\ v_\psi &= \widehat{k} \times \nabla \psi, \\ \nabla^2 \chi &= \delta, \\ v_\chi &= \nabla \chi, \\ v_g &= \widehat{k} \times \nabla \phi, \end{aligned} \tag{1}$$

where ψ, ζ, v_ψ, χ, δ, and v_χ represent the stream function, relative vorticity, nondivergent wind, velocity potential, horizontal divergent, and divergent wind, respectively. Once the divergent wind is calculated, it is subtracted from the first-guess U and V wind fields. Next, the geopotential height anomaly, the geostrophic wind, and temperature anomaly are subtracted from the first-guess field. Finally, the surface and sea-level pressure perturbations are subtracted. So, only the background flow where the first-guess storm was originally located is left.

2.3. Numerical Simulation Settings. With the purpose of studying the one-way influence of the interaction mode for typhoons Tembin and Bolaven, the advanced Weather Research and Forecasting Model (WRF, V3.6) is used for the numerical simulation. The model integration time is from 1200 UTC 23 August to 1200 UTC 27 August 2012. Euler mass coordinate, Runge–Kutta 3rd-order time integration option, and two-way nesting with double-nested grids are applied. The model is centered at 28.0°N, 125.0°E with horizontal resolutions of 27 km for D01 and 9 km for D02, 31 eta levels in the vertical direction, and a model top level at 50 hPa. The model configurations include a 241×203 grid in the outer nest (D01) and a 268×274 grid in the inner nest (D02). The physical parameterization schemes used in the numerical simulation include the WRF single-moment 6-class microphysics scheme [14], the rapid radiative transfer model longwave radiation scheme [15], the Dudhia

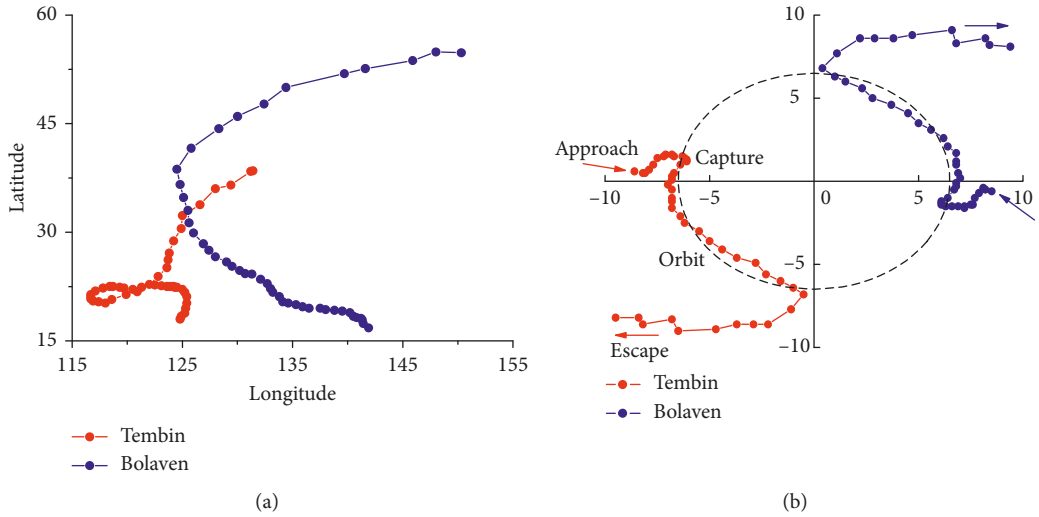

FIGURE 1: Tracks of Typhoons Tembin and Bolaven (a) and a "Fujiwhara" diagram for the binary interaction between them (b) from 0000 UTC 20 August to 0000 UTC 1 September (interval: 6 hours; red dots: Tembin; blue dots: Bolaven). In (b), distances are in degrees latitude. Dots are centroid-relative positions. The major elements of "Approach", "Capture", "Orbit", and "Escape" are labelled. The radius of dash circle is 6.5 degrees. The origin of coordinate denotes the geographical center between the two vortices.

shortwave radiation scheme [16], the unified Noah land-surface model land-surface scheme [17], the Yonsei University planetary boundary layer scheme [18], and the Kain–Fritsch convective scheme [19]. The experiment setting above is denoted as CTL experiment. To remove the Tembin and Bolaven vortices, TC bogus scheme provided by the WRF modeling system is applied for the sensitivity experiments (denoted as NoT experiment and NoB experiment, respectively) with the same experiment settings as the CTL experiment.

3. Results and Discussion

3.1. Synoptic Situation Analysis. The synoptic evolution was shown by the 500 hPa geopotential height fields from the European Centre for Medium-Range Weather Forecasts (ECMWF) ERA-Interim reanalyses data from 0000 UTC 24 August to 0000 UTC 27 August (Figure 2). There were one trough and one ridge in midhigh latitudes regions locating in China and Japan, respectively. The circulation center of subtropical high (the contour of 576 dagpm) was located in the ocean and extended westward from 0000 UTC 24 August to 0000 UTC 25 August, with the westernmost contours of 576 dagpm locating at 110°E. During this time, the two TCs moved westward along the periphery of the subtropical high and the distance between typhoons Tembin and Bolaven gradually became smaller. After 0000 UTC 26 August, the trough started to deepen and move eastward and the intensity of the subtropical high weakened with its main body retreating eastward and stretching southward in a meridional pattern. During this period, Tembin moved southward and then turned northeastward, and Bolaven constantly moved northward. It should be noticed that when Tembin made a looping track, i.e., from 0000 UTC 25 August to 1200 UTC 27 August, its translation speed was slower than Bolaven's. To clearly describe the behaviour of interacting tropical vortices, the centroid-relative motion for the two typhoons is displayed in Figure 1(b). The two TCs started to approach the centroid at 0000 UTC 20 August, and a sudden onset of cyclonic orbit occurred after 1800 UTC 22 August, followed by a sudden capture. The distance between the two TCs tended to become slightly larger, and a period of stable cyclonic orbit began at 0600 UTC 26 August and ended at 0600 UTC 28 August. A sudden escape occurred when the separation distance gradually became larger after 0600 UTC 28 August.

At the point of interest, typhoons Tembin and Bolaven started to cyclonically orbit when the separation distance was about 800 miles (the dash circle in Figure 1(b) indicates Brand's typical cyclonic-orbit onset distance of 750 miles, about 13 degrees in latitude). In addition, the actual orbit track was not distinctly cyclonically curved. These characteristics indicate that the tracks of typhoons Tembin and Bolaven were likely to be affected by the monsoon over the western North Pacific. To verify that, an experiment (denoted as NoM experiment) applying a low-pass Lanczos filter with a 10-day cutoff period to the wind fields to remove the low-frequency flows (original fields minus the result from the low-pass Lanczos filter) [20] is carried out to determine the binary interaction behaviour in the absence of the monsoon. The results will be discussed in Section 3.3.

3.2. Simulation Verification. The best track data from the Japan Meteorological Agency (JMA) and Joint Typhoon Warning Center (JTWC) are used to verify the simulation results of the track and intensity of the two typhoons. As shown in Figure 3, the model succeeded well in simulating the tracks of Tembin and Bolaven in the CTL experiment, especially Tembin's looping track, but the translation speed of the two typhoons (in white circle) was faster than the best track. On the other hand, as shown in Figure 4, although the

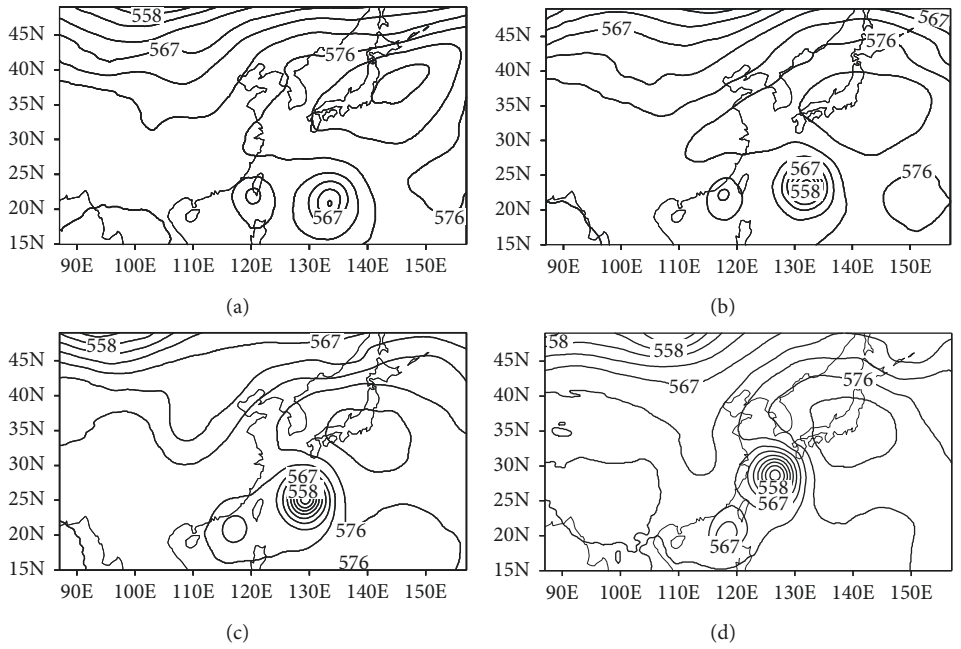

Figure 2: Geopotential height at 500 hPa based on the ECMWF reanalysis data at 0000 UTC 24 August (a), 0000 UTC 25 August (b), 0000 UTC 26 August (c), and 0000 UTC 27 August (d) (intervals: 3-dagpm).

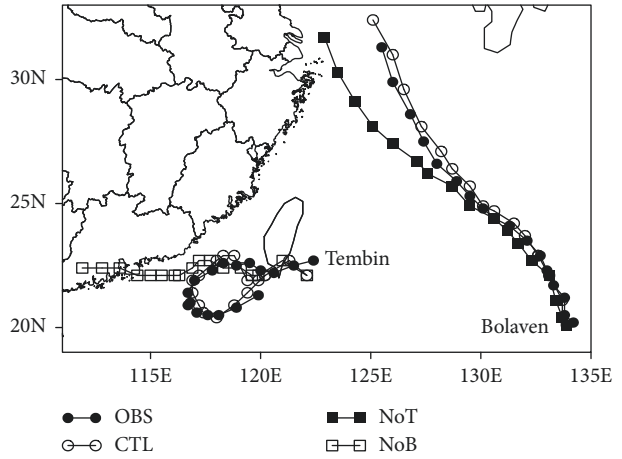

Figure 3: Tracks of Tembin and Bolaven from 1200 UTC 23 August to 1200 UTC 27 August (interval: 6 hours; black circle track: JTWC best track; white circle track: CTL experiment; black square track: NoT experiment; white square track: NoB experiment).

differences in the minimum sea-level pressure (MSLP) and maximum surface wind speed (MSWS) from the JMA and JTWC were significant, even at the initial time, the evolutionary trends of the MSLP and MSWS were nearly the same. The intensity evolutionary trends of the two typhoons in the CTL experiment were successfully recreated by the numerical simulation. Note that because the model initial condition was modified in the two sensitivity experiments, the model was unstable at the first 24 h integration time. Therefore, the verification of the two sensitivity experiments using the TC bogus scheme (NoT and NoB experiments) is shown by the multiple levels at 1200 UTC 24 August (Figure 5). The vortex of Tembin was removed completely at the sea level and 500 hPa isobaric level. However, there was still weak circulation of Bolaven at the sea level after applying the TC bogus scheme. The reason for that may be due to the size of Bolaven which was much bigger, and the scheme could not remove this size of vortex completely. All in all, this left-over vortex of Bolaven (actually, it was the remnant of monsoon which will be discussed in Section 3.3) in the NoB experiment had little impact on the Tembin since its intensity was much weaker.

3.3. Binary Typhoon Track. The tracks of Tembin and Bolaven in the two sensitivity experiments are shown in Figure 3. It is remarkable that Tembin made a steady westward movement in the NoB experiment, which was completely different from the observations. Compared with the observations, Bolaven shifted westward in the NoT experiment after 0000 UTC 26 August, which was likely to make a greater influence on eastern China. On the other hand, Tembin made an evident southward motion in the NoM experiment without the monsoon obstructing it to move south as compared with observations and the CTL experiment (Figure 6(a)), and the orbit path for the TCs was more cyclonically curved (Figure 6(b)). Meanwhile, the translation speed of Bolaven was greatly reduced in the NoM experiment (Figure 6(a)). The southwesterly low-level jet (wind speed over 12 m s^{-1} in Figure 6(f)) to the south and southeast of the TCs was removed in the NoM experiment so that the circulations of the two TCs both became smaller. Also, the strength of the anticyclone circulation in the south of the TCs was weaker than that of the CTL (Figure 6(c)) and NoT experiments (Figure 5(f)), and the subtropical high in the north of the TCs was divided into two parts with one locating over the Eastern China and the other locating over

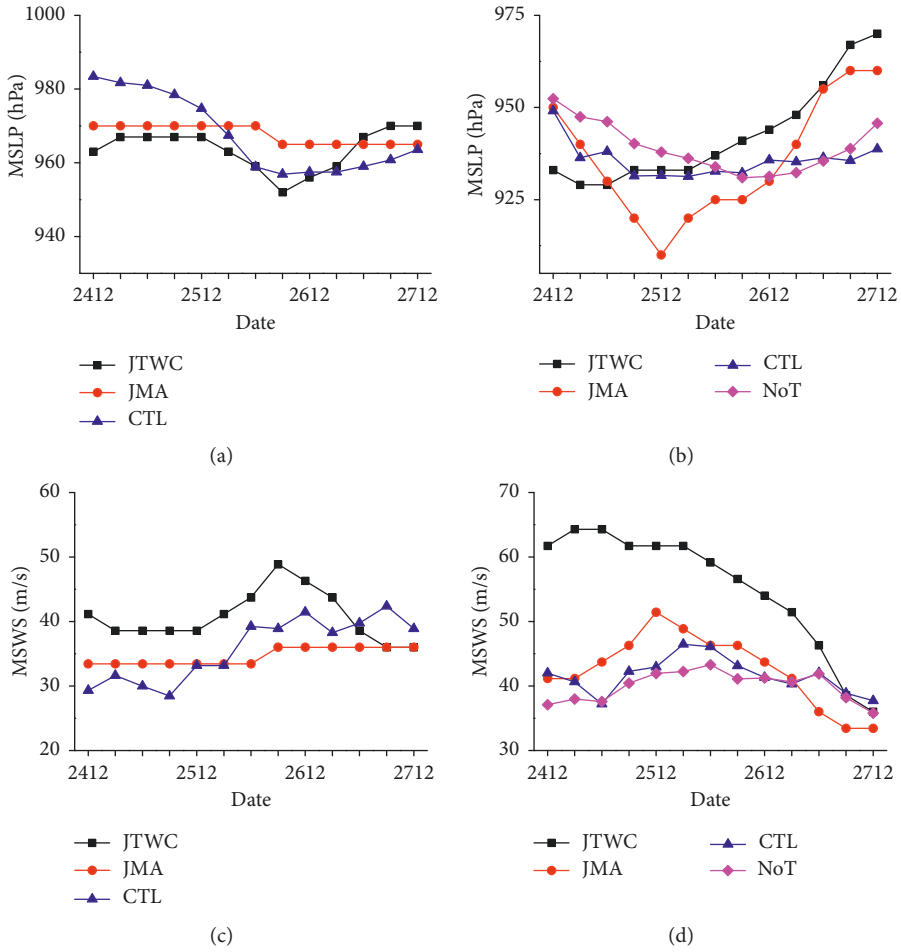

FIGURE 4: Time series of the MSLP (unit: hPa) and the MSWS (unit: m s^{-1}) of Tembin (a, c) and Bolaven (b, d) from 1200 UTC 24 August to 1200 UTC 27 August, respectively (unit: hPa; square line: JTWC best track; circle line: JMA best track; triangle line: CTL experiment; diamond line: NoT experiment).

Japan (Figure 6(d)). Under this synoptic situation, Bolaven moved northward much more slowly as the steering flow was not distinct. These results suggest that the monsoon had an impact on both the tracks and the translation speeds of the TCs, especially for the smaller vortex of Tembin which was also affected by both the existence of Bolaven. It is worth mentioning that the left-over vortex in the NoB experiment was the remnant of monsoon which was broad and belonged to the low-frequency flows and the TC bogus scheme could not completely remove it.

Many previous researches have demonstrated that the environmental steering flow has best correlation with TC motion [21–26]. To access the differences in the trajectories of the two typhoons in the CTL and the two sensitivity experiments, the environmental steering flow is calculated as the deep-layer mean (from 850 hPa to 300 hPa) wind averaged over a 5°–7° annulus around the TC's center, that is, the steering flow at each level is

$$V(p) = \frac{\int_5^7 \int_0^{2\pi} V r \, dr \, d\theta}{\int_5^7 \int_0^{2\pi} r \, dr \, d\theta}, \quad (2)$$

and the deep-layer-mean steering flow is

$$V_{\mathrm{DLM}} = \frac{\int_{850}^{300} V(p) dp}{\int_{850}^{300} dp}, \quad (3)$$

where V is the meridional component V_x or the zonal component V_y of the environmental steering flow. As seen in Figure 7, the evolution of the environmental steering flow was generally consistent with that of the translation speed of the two TCs in all experiments. For Typhoon Bolaven (Figures 7(a) and 7(b)), the variations in the environmental steering flow and the TC translation speed were both small except that the zonal component of the translation speed was a little higher in the NoT experiment. Without the existence of Typhoon Tembin, the westward component of the translation speed of Bolaven started to increase after 0000 UTC 25 August, which corresponded to the westward movement of Bolaven in the NoT experiment. For Typhoon Tembin (Figures 7(c) and 7(d), the environmental steering flow and the translation speed were greatly different in the CTL and NoB experiments. The zonal component of the environmental steering flow and TC translation speed shifted eastward after 0000 UTC 25 August in the CTL run while it remained westward in the NoB run. The meridional

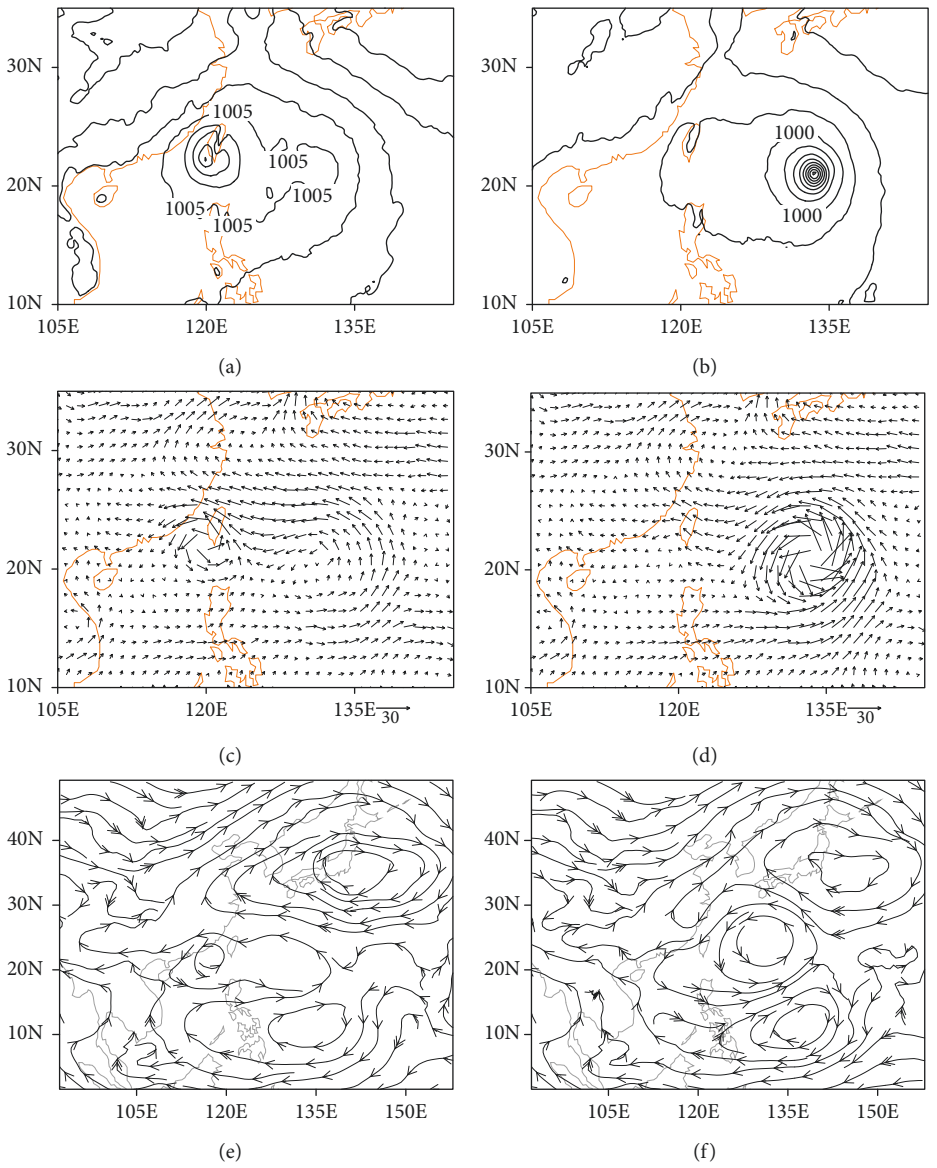

Figure 5: Sea-level pressure ((a, b), interval: 5 hPa) and wind vector at 500 hPa (c, d) at 1200 UTC 24 August as well as streamline at 500 hPa at 0000 UTC 25 August (e, f) in the NoB (a, c, e) and NoT experiments (b, d, f), respectively.

component of the environmental steering flow was northward in the NoB experiment but remained southward in the CTL experiment during 0000 UTC 25 August to 1200 UTC 26 August. These results suggest that, without the existence of Bolaven, the surrounding atmosphere was altered a lot, making a different track of Tembin in the NoB experiment as compared with the observations; but the influence of Tembin on the track of Bolaven was slight with minor difference in tracks in the CTL and NoT experiments. Meanwhile, the monsoon circulation made a contribution to both the tracks and the translation speeds of Tembin and Bolaven as discussed above.

A PV tendency diagnostic approach proposed by Wu and Wang [27] was applied to evaluate the TC motion in this study. Previous studies [28, 29] have shown that the PV tendency was useful to diagnose the track of TC, especially the anomaly track, indicating that TC moves to the region where the PV tendency reaches maximum. The PV and the vorticity equation in the pressure coordinate can be expressed, respectively, as

$$P = -g\left[(\zeta + f)\frac{\partial\theta}{\partial p} + \frac{\partial u}{\partial p}\frac{\partial\theta}{\partial y} - \frac{\partial v}{\partial p}\frac{\partial\theta}{\partial x}\right], \tag{4}$$

$$\frac{d(\zeta + f)}{dt} = -(\zeta + f)\left(\frac{\partial u}{\partial x} + \frac{\partial v}{\partial y}\right) + \left(\frac{\partial\omega}{\partial y}\frac{\partial u}{\partial p} - \frac{\partial\omega}{\partial x}\frac{\partial v}{\partial p}\right) + \frac{\partial F_y}{\partial x} - \frac{\partial F_x}{\partial y}, \tag{5}$$

where P, g, θ, ζ, and f are the potential vorticity, gravitational acceleration, potential temperature, relative vorticity, and the Coriolis parameter, x, y, and p are the zonal, meridional,

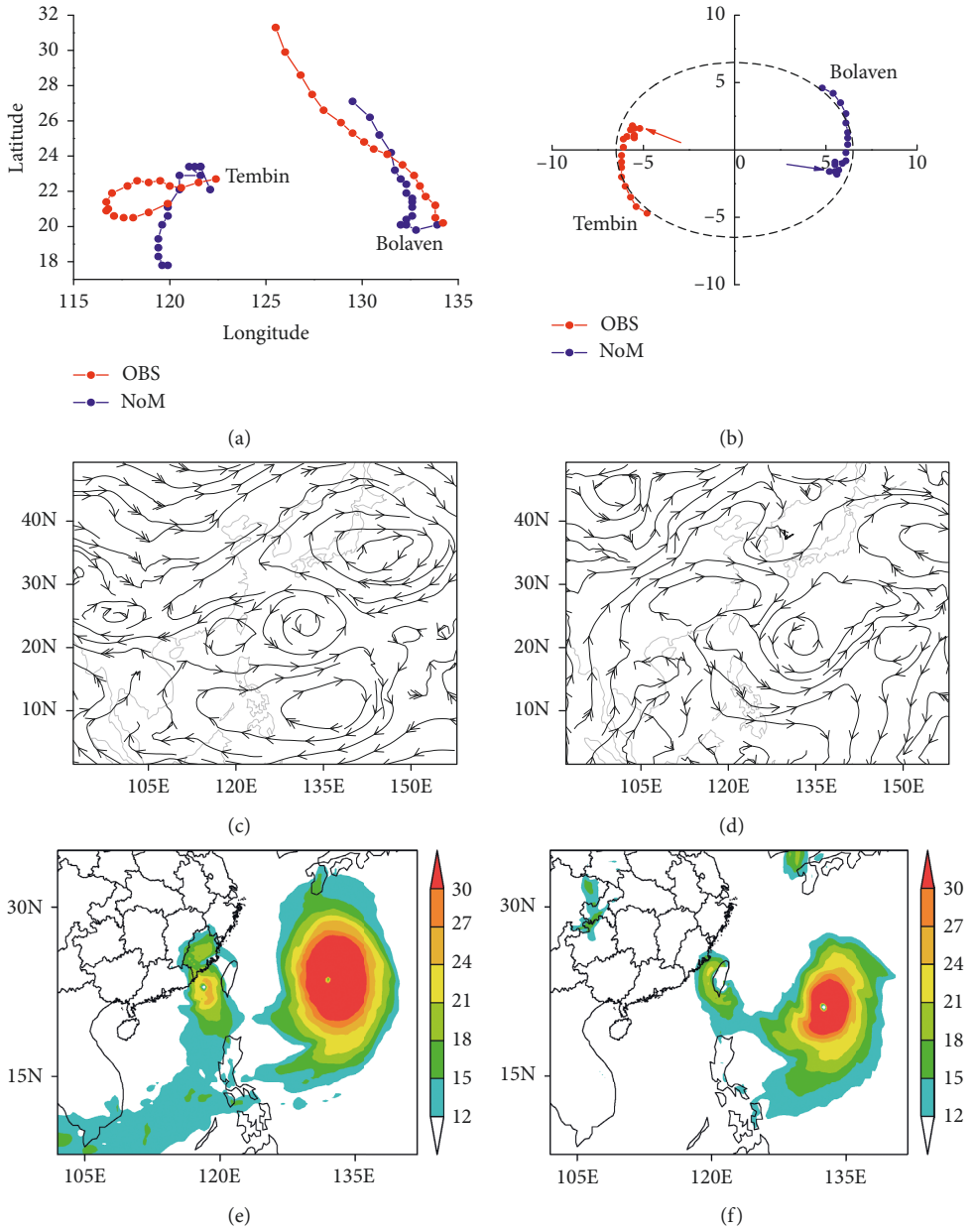

FIGURE 6: Tracks of Typhoons Tembin and Bolaven (a) and a "Fujiwhara" diagram for the binary interaction between them (b) in the NoM experiment from 1200 UTC 23 August to 1200 UTC 27 August (interval: 6 hours; red dots: Tembin; blue dots: Bolaven). In (b), distances are in degrees latitude. Dots are centroid-relative positions. The radius of dash circle is 6.5 degrees. The origin of coordinate denotes the geographical center between the two vortices. The 500 hPa streamline at 0000 UTC 25 August as well as the 850 hPa wind fields (interval: 3 m s^{-1}) in the CTL (c, e) and NoM experiments (d, f).

and pressure coordinates, u, v, and ω are the wind components in the x, y, and p directions, and F_x and F_y are the friction component in the x and y directions. Differentiating equation (4) with respect to time yields, we get

$$\frac{dP}{dt} = -g\left[\frac{\partial\theta}{\partial p}\frac{d(\zeta+f)}{dt} + (\zeta+f)\frac{d}{dt}\left(\frac{\partial\theta}{\partial p}\right) + \frac{d}{dt}\left(\frac{\partial u}{\partial p}\frac{\partial\theta}{\partial y} - \frac{\partial v}{\partial p}\frac{\partial\theta}{\partial x}\right)\right]. \quad (6)$$

Substituting equations (5) into (6), the PV tendency (PVT) equation can be written as

$$\frac{\partial P}{\partial t} = F_1 + F_2 + F_3 + F_4, \quad (7)$$

where F_1 represents the horizontal PV advection,

$$F_1 = -u\frac{\partial P}{\partial x} - v\frac{\partial P}{\partial y}, \quad (8)$$

F_2 represents the vertical PV advection,

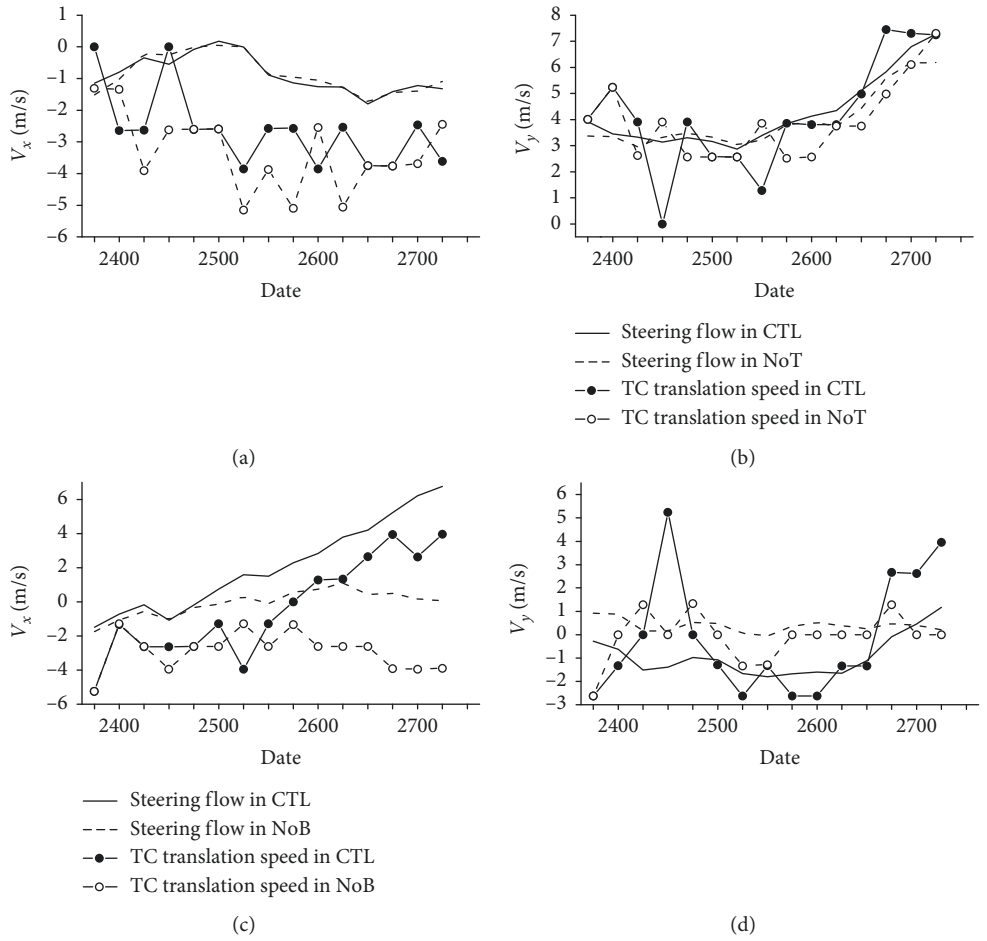

Figure 7: Time series of the zonal component (a, c) and the meridional component (b, d) of the environmental steering flow (solid line: CTL experiment; dash line: sensitivity experiments) and the translation speed (black circle line: CTL experiment; white circle line: sensitivity experiments) of Bolaven (a, b) Tembin and (c, d) from 1800 UTC 23 August to 1200 UTC 27 August (unit: m s^{-1}).

$$F_2 = -\omega \frac{\partial P}{\partial p}, \tag{9}$$

F_3 represents the diabatic heating,

$$F_3 = -g\left[(\zeta + f)\frac{\partial}{\partial p}\left(\frac{d\theta}{dt}\right) + \frac{\partial u}{\partial p}\frac{\partial}{\partial y}\left(\frac{d\theta}{dt}\right) - \frac{\partial v}{\partial p}\frac{\partial}{\partial x}\left(\frac{d\theta}{dt}\right)\right], \tag{10}$$

F_4 represents the friction,

$$F_4 = -g\left[\left(\frac{\partial F_y}{\partial x} - \frac{\partial F_x}{\partial y}\right)\frac{\partial \theta}{\partial p} + \frac{\partial F_x}{\partial p}\frac{\partial \theta}{\partial y} - \frac{\partial F_y}{\partial p}\frac{\partial \theta}{\partial x}\right]. \tag{11}$$

Equation (7) suggests that the PV tendency results from horizontal (HA) and vertical (VA) PV advection, diabatic heating (DH), and friction. HA represents that the external large-scale circulation contributes to the PVT, and DH represents that the PV is affected by the internal convective activity of TC. Since the VA is smaller than any other terms in the PVT equation and TC mainly moves over ocean, the contributions from the VA and friction are ignored in this study. The vertical integrated HA, DH, and PVT in the air column are calculated and used to evaluate the different tracks of Tembin in the CTL and NoB experiments. In the CTL experiment, the distribution of PVT was northeast-southwest direction at 0600 UTC 25 August (Figure 8(c)) and after that time, the distribution turned to south-north direction. During this period, Tembin moved from westward to southward (black dot represents the current TC's position, and purple dot represents the next 6 h TC's position), which indicates that Tembin tended to move to the regions with maximum positive PVT and the change in Tembin's track was correctly reflected by the change in the PVT distribution. Note that the pattern of HA was consistent with that of PVT but the distribution of DH was asymmetric and the order of magnitude was smaller, suggesting that the contribution from the DH to the PVT was smaller than that of the HA. At 1800 UTC 26 August, the distributions of PVT, HA, and DH were both turned to east-west direction and Tembin moved eastward (Figures 8(d)–8(f)). After that time, the distribution of DH became symmetric (Figure 8(h)), and the environmental steering flow and the translation speed started to increase gradually (Figures 7(c) and 7(d). In the NoB experiment, the distributions of PVT and HA were nearly the same with the results from the CTL experiment before 0600 UTC 26

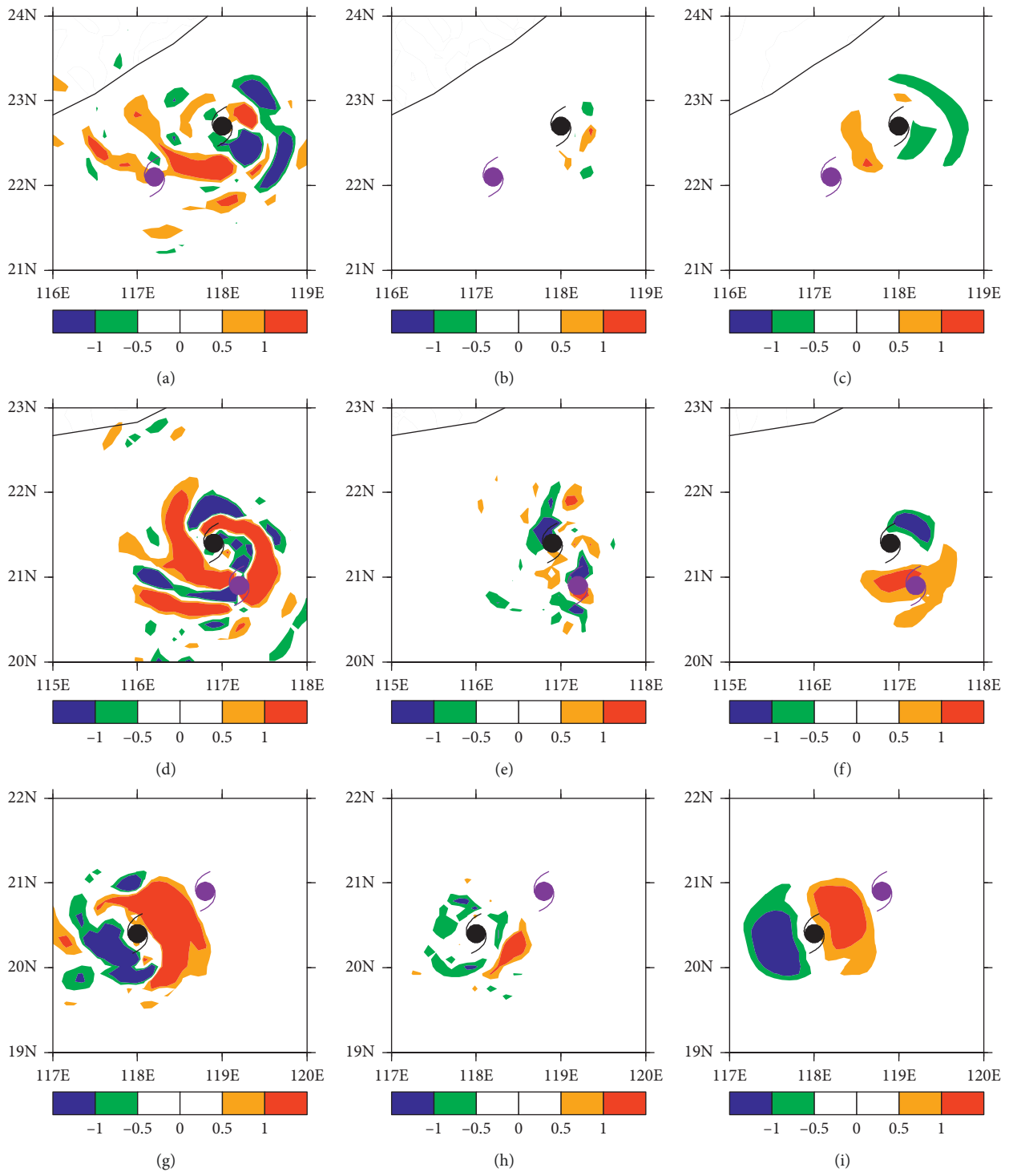

Figure 8: Vertical integrals of horizontal PV advection (HA (a, d, g)), diabatic heating (DH (b, e, h)), and PV tendency (PVT (c, f, i)) in the CTL experiment at 0600 UTC 25 August (a–c), 0000 UTC 26 August (d–f), and 1800 UTC 26 August (g–i). Black dot represents the current Tembin's position and purple dot represents the next 6 h Tembin's position (unit: 10^{-6} K m^2 kg^{-1} s^{-2}).

August (Figures 9(a) and 9(c)). However, the distributions of them turned to east-west direction after that time (Figures 9(d) and 9(f), and Tembin moved westward steadily (Figure 3), which was distinctly different to the results from the CTL experiment (Figures 8(d) and 8(f)). During this period, the distribution of DH was asymmetric (Figures 9(b) and 9(e)), which restrained the westward movement of Tembin, making its translation speed decrease from 1200 UTC 25 August to 1200 UTC 26 August. The influence of DH on the track of Tembin reduced after 1800 UTC 26 August with the magnitude of DH decreasing sharply (Figure 9(h)).

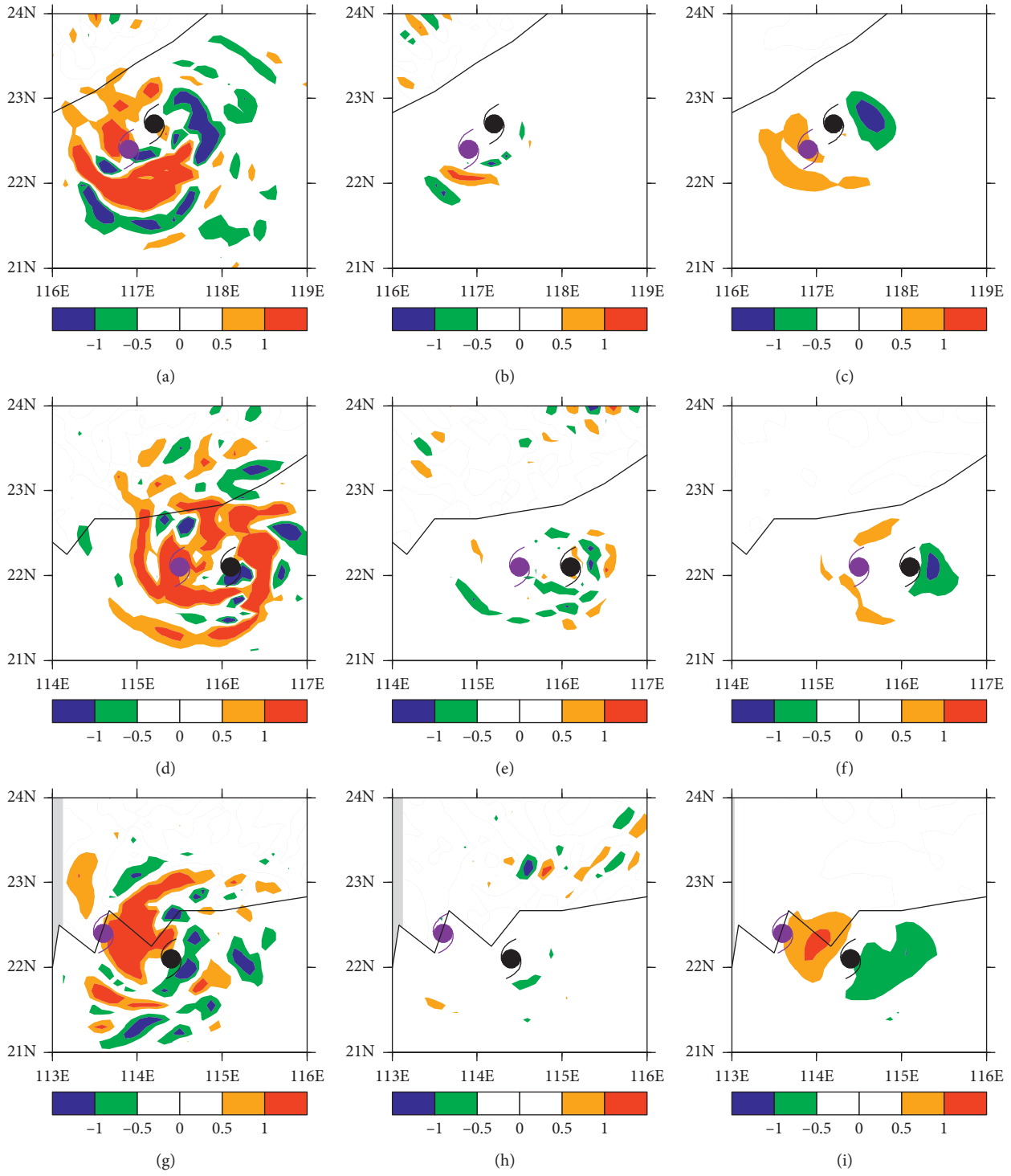

Figure 9: Vertical integrals of horizontal PV advection (HA, (a, d, g)), diabatic heating (DH (b, e, h)), and PV tendency (PVT (c, f, i)) in the NoB experiment at 0600 UTC 25 August (a–c), 0000 UTC 26 August (d–f), and 1800 UTC 26 August (g–i). Black dot represents the current Tembin's position, and purple dot represents the next 6 h Tembin's position (unit: $10^{-6}\,\mathrm{K\,m^2\,kg^{-1}\,s^{-2}}$).

Compared with the results from the CTL experiment, the HA made a dominant and promotional influence on the PVT; in other words, the looping track of Tembin was mainly caused by the impact of the large-scale environmental flow. The existence of the monsoon and Bolaven altered the environmental flow, which was also clearly shown in Figures 6(c) and 6(d) and Figures 5(e) and 5(f). The southerly greatly reduced in the south of Bolaven in the absence of the monsoon (Figure 6(d)). When Bolaven moved poleward with increasing intensity, the formation of the south side of the subtropical high began to alter and its ridge line moved southward (Figure 6(c)), which was

evidently observed in the NoT experiment (Figure 5(f)). However, the ridge line of the subtropical high was a constant east-west direction in the NoB experiment (Figure 5(e)) and the corresponding environmental steering flow of Tembin (Figures 7(c) and 7(d)) was northwestward, making Tembin move westward steadily.

3.4. Binary Typhoon Intensity. The area of the water vapor associated with the southwesterly flow over the South China Sea in the CTL run was larger than that in the NoT run. It suggests that Tembin had an ability to drag considerable amount of water vapor from the South China Sea. And, there was air flow between the two typhoons in the CTL experiment (Figure 10). Obviously, the water vapor carried by the southwesterly flow was divided into two parts, where one was absorbed by Tembin and the other became one of Bolaven's water vapor sources. However, Tembin was located at upstream of the southwesterly, which interrupted part of the water vapor being transported to Bolaven with few water vapor inflow as compared with that in the NoT run. Simultaneously, the distribution of the water vapor flux near Bolaven's center in the NoT experiment was more symmetrical than that in the CTL run. These results suggest that the existence of Tembin was not conducive to the supply of water vapor to Bolaven.

The simulation results of the intensity of Bolaven in the CTL and NoT experiment (the diamond line in Figures 4(b) and 4(d) showed that Bolaven's intensity was higher after 1200 UTC 24 August but lower after 0000 UTC 27 August. These differences in the intensity of Bolaven indicate that the existence of Tembin seemed to have an impact on the intensity of Bolaven, which is discussed below.

Bolaven intensified simultaneously with the magnitude of wind in low troposphere, which was directly reflected by the increased kinetic energy. The kinetic energy budget is used to investigate the reason for the variations of the intensity of Bolaven in the CTL and NoT experiments. The kinetic energy budget can be expressed as [30]

$$\frac{\partial K}{\partial t} = -V_{\mathrm{h}} \cdot \nabla\phi - \nabla \cdot K\left(V_{\mathrm{h}} - C_{\mathrm{tc}}\right) - \frac{\partial K\,\omega}{\partial p} + V_{\mathrm{h}} \cdot F, \quad (12)$$

where $K = (1/2)(u^2 + v^2)$ is the horizontal kinetic energy per unit mass of air parcel, V_{h} is the horizontal wind vector, C_{tc} is the translation vector of Bolaven, and F is the friction. Simplifying equation (12) results in

$$\frac{\partial K}{\partial t} = G_{\mathrm{k}} + HF_{\mathrm{k}} + VF_{\mathrm{k}} + R. \quad (13)$$

The left-hand side represents the local rate of change in kinetic energy per unit mass of air parcel. The terms on the right-hand side represent the ways in which kinetic energy can be changed and include the generation of kinetic energy (G_{k}), horizontal flux of kinetic energy (HF_{k}), vertical flux of kinetic energy (VF_{k}), and kinetic energy dissipation (R) due to friction. The temporal evolution of kinetic energy budget terms in the CTL and NoT experiments shows that the local rate of change in kinetic energy was basically positive, indicating that the intensity of Bolaven increased gradually. And, the major contribution to the kinetic energy increase in low troposphere came from G_{k} and to the kinetic energy dissipation came from VF_{k} (not shown). The differences in the kinetic energy budget terms between the CTL and NoT experiments are represented in Figure 11. The magnitude of positive values of G_{k} was bigger in the NoT experiment during the investigating period (Figure 11(a)), suggesting that the source of kinetic energy, that is, the available potential energy converted into kinetic energy by pressure gradient force, was greater than that in the CTL experiment. HF_{k} reflects the kinetic energy exchange between Bolaven and the surrounding atmosphere. The significant differences in HF_{k} between the two experiments were observed in low troposphere (below 850-hPa) (Figure 11(b)), which was related to the variations in the low-level jet. A considerable amount of energy was transported out of the area of Bolaven by HF_{k} whose values were negative below 900 hPa in both experiments after 1200 UTC 24 August, and this kinetic energy output was higher in the CTL experiment from 1200 UTC 24 August to 0000 UTC 26 August. Above 900 hPa, HF_{k} was positive in the NoT experiment during the entire period, but its magnitude was smaller after 0000 UTC 27 August. These results suggest that the existence of Tembin tended to hamper the kinetic energy being transported to Bolaven by the low-level jet, which corresponded to the analyses of water vapor flux (Figure 10). VF_{k} represents the vertical transport of kinetic energy from low levels to upper levels, and negative values found in both experiments in the low layer (950–700 hPa) dominate throughout the period (not shown). It indicates that the transport of kinetic energy aloft by the ascending motion was the source of kinetic energy to the upper layer (100–300 hPa) with the positive values of VF_{k}. The frictional dissipation effect in both experiments was produced below 850 hPa; however, the positive values of R were found at the layer between 850 hPa and 300 hPa during the entire time. The positive values indicate that a transfer of energy from subgrid to grid scales of motion is a source of kinetic energy, which was reported by previous studies [31–33]. At certain moments, such as active convection and mutual stage of TC, the conversion of kinetic energy in a subgrid scale to that in the grid scale could be a source of kinetic energy and the values of R could be positive. The positive values of R observed in middle troposphere reflect the contribution from active convection to the increase in the kinetic energy at the upper level. Note that, as shown in Figure 11, the main differences in the kinetic energy budget terms were both occurred from 0000 UTC 26 August to 0000 UTC 27 August in the low layer (950–850 hPa). The contributions from the kinetic energy budget terms in the NoT experiment seem to be more beneficial to the development of Bolaven, for example, more kinetic energy was generated by G_{k} in low troposphere (Figure 11(a)), and more kinetic energy was transported to the upper troposphere by ascending motion (Figure 11(c)). But, actually, the intensity of Bolaven was weaker than that in the CTL experiment except after 0000 UTC 26 August.

A series of observations and numerical simulations have shown that vertical wind shear has an important effect on TC

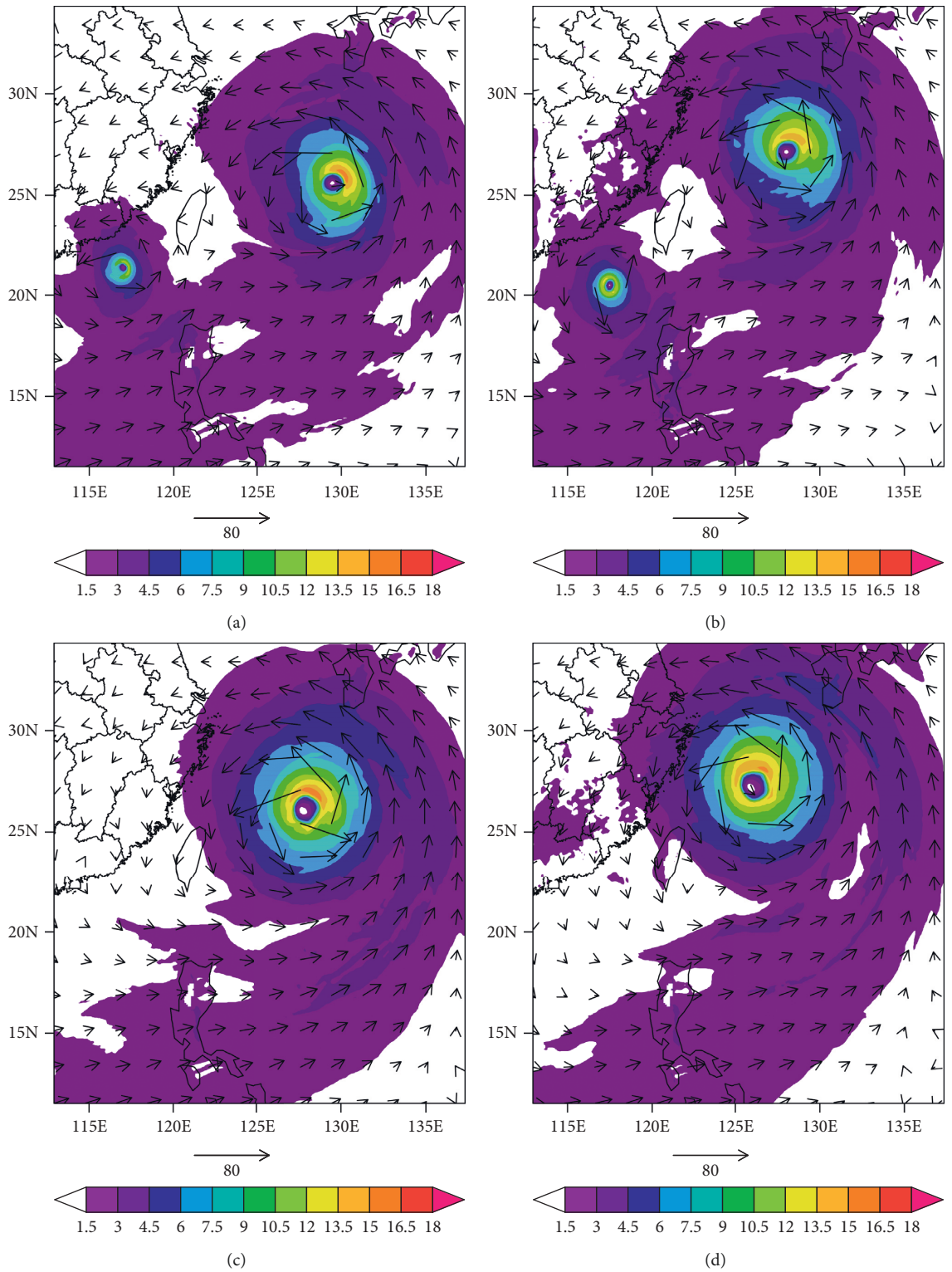

FIGURE 10: The 850 hPa water vapor flux (shaded) at 0000 UTC 26 August (a, c) and 1200 UTC 26 August (b, d) in the CTL experiment (a, b) and the NoT experiment (c, d) (unit: $kg\,hPa^{-1}\,m^{-1}\,s^{-1}$).

intensity [34–38]. The area-averaged (1000 km × 1000 km) horizontal winds over Bolaven and the area-averaged (1000 km × 1000 km) magnitude of deep-layer shear vector between 200 hPa and 850 hPa, as well as the low-layer shear vector between 850 hPa and 1000 hPa, were calculated to investigate the reason why the intensity of Bolaven was weaker in the NoT experiment before 0000 UTC 26 August. The results (Figure 12) show that the magnitude of the

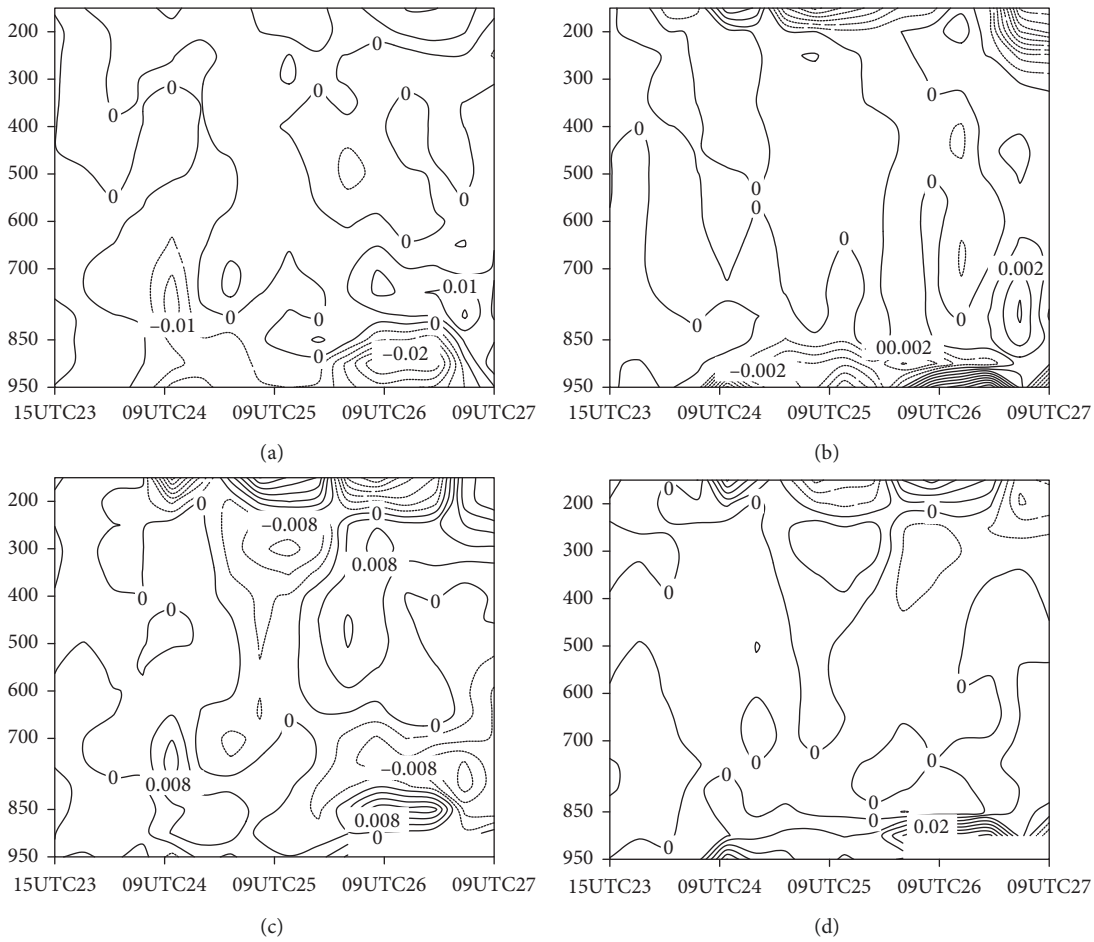

FIGURE 11: Height-time sections of kinetic energy budget terms (unit: $m^2\ s^{-3}$): generation kinetic energy (a), horizontal flux of kinetic energy (b), vertical flux of kinetic energy (c), and kinetic energy dissipation (d) from 1500 UTC 23 August to 0900 UTC 27 August.

averaged horizontal wind at lower levels were evidently greater in the NoT experiment than in the CTL run (Figures 12(a) and 12(b)). Although the difference in the wind direction at all levels in the two experiments was minor, the low-layer shear was stronger than that in the CTL experiment due to an increase in wind speed at low levels in the NoT experiment. Note that the low-layer shear and the deep-layer shear in the NoT experiment were both greater as compared with the results from the CTL experiment from 1200 UTC 24 August to 0000 UTC 26 August (Figures 12(c) and 12(d)). The upper circulation would be blown away from the low-level center of TC due to a stronger vertical wind shear, which is highly not conducive to the development of ascending motion and the intensity of TC. As shown in Figure 11(c), the magnitude of negative values of VF_k in the middle and upper layers (800–300 hPa) was bigger in the CTL experiment than in the NoT experiment before 0000 UTC 26 August, indicating that the ascending motion was so strong that more kinetic energy was transported to the upper level, especially at 1200 UTC 25 August. After that time, the vertical wind shear weakened in the NoT experiment (Figures 12(c) and 12(d)) and the strength of ascending motion became stronger so that more kinetic energy was transported to the upper levels (Figure 11c) and the intensity of Bolaven became stronger (Figures 4(b) and 4(d)).

4. Conclusions

The binary typhoon effect is a challenge in typhoon research because of its difficulty to predict. Previous studies on how the one-way interaction mode works is still unclear, such as the case of typhoons Morakot and Goni in 2009. In this report, a typical case of one-way interaction type, typhoons Tembin and Bolaven, was analyzed to investigate the binary typhoon effect on the track and intensity of the two typhoons by using the WRF model. The results are as follows:

(1) The tracks of Tembin and Bolaven were diagnosed by the environmental steering flow, showing that there was a good relationship between the environmental steering flow and the tracks of the two TCs. And, the impact of the existence of Tembin on the track of Bolaven was negligible due to relatively slight differences in the environmental steering flow and translation speed of Bolaven. However, the results from the potential vorticity tendency demonstrated that Tembin tended to move to the region with

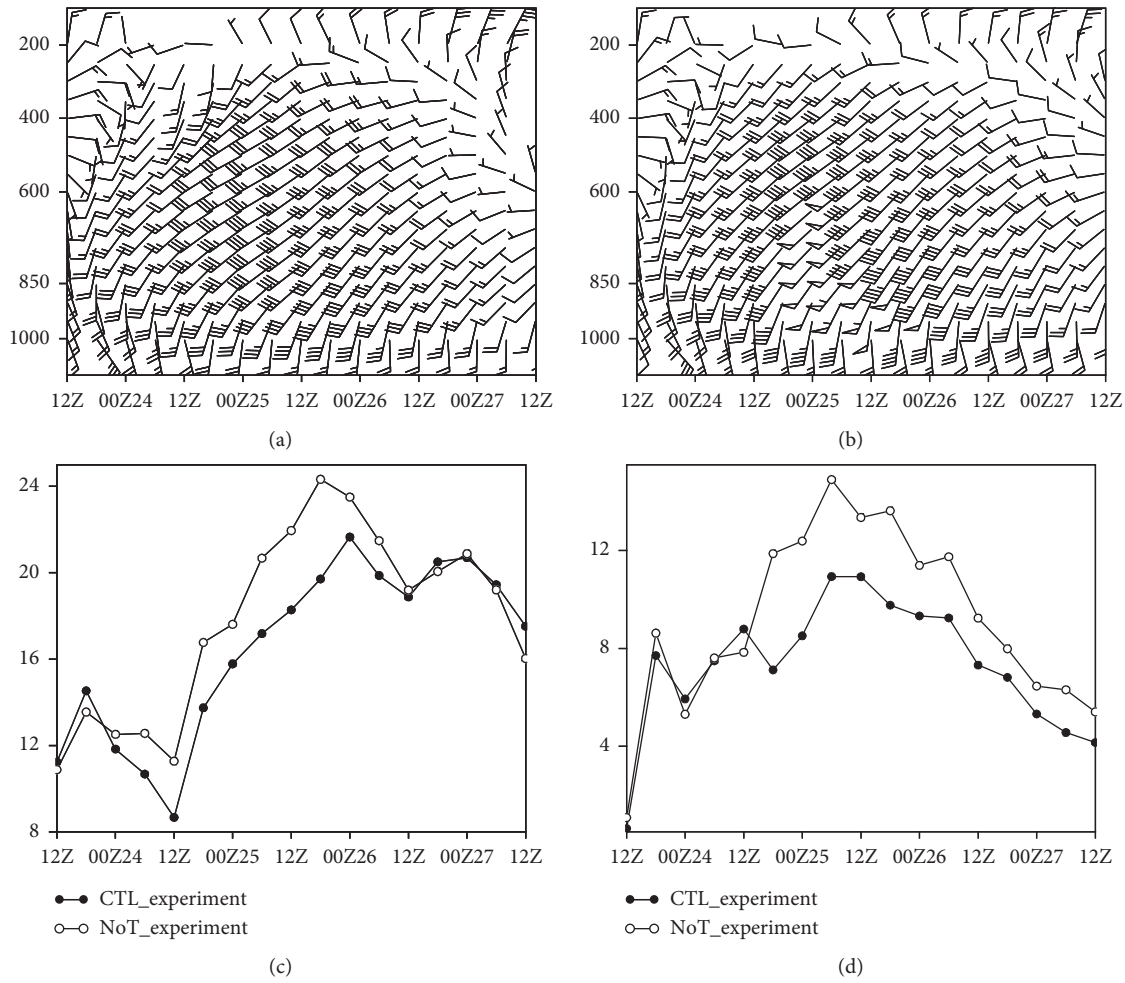

Figure 12: The simulated pressure-time cross sections of the area-averaged (1000 km × 1000 km) horizontal winds over Typhoon Bolaven ((a) CTL experiment and (b) NoT experiment) and time series of the area-averaged (1000 km × 1000 km) magnitude of the simulated deep-layer shear vector (c) and low-layer shear vector (d) in the CTL experiment (black circle line) and NoT experiment (white circle line), respectively (unit: m s^{-1}).

maximum positive PVT and the main contributions to its looping track were the horizontal PV advection. In other words, the track of Tembin was affected by the external surrounding circulation associated with Bolaven. In addition, the monsoon over the western North Pacific also affected the tracks and the translation speeds of the TCs, especially for the smaller vortex of Tembin, which makes the tracks of TCs more complex.

(2) The analysis of kinetic energy budget suggests that the development of Bolaven owed to the generation of kinetic energy in low troposphere and the vertical transport of kinetic energy to upper troposphere. The existence of Tembin not only interrupted the water vapor being transported to Bolaven but also affected the strength of vertical wind shear. Without the vortex of Tembin, the relatively bigger magnitude of the low-layer and deep-layer wind shear was not conducive to the vertical transport of kinetic energy by ascending motion, resulting in the much weaker intensity of Bolaven during the looping track of Tembin.

This study demonstrates clearly the mechanisms of the one-way interaction mode that affects the track and intensity of binary typhoons. These conclusions can also shed some light on the improvement of the TC prediction when the binary typhoon effect occurs. More work related to other typical categories in binary typhoon effect research could be done in the future, such as merging cases to illustrate the physical mechanisms of binary typhoon systems in more detail.

Data Availability

Most of the data series used to support the findings of this study are obtained from the Research Data Archive, which is available on the web at https://rda.ucar.edu/. The European Centre for Medium-Range Weather Forecasts (ECMWF) ERA-Interim reanalyses data are also available on the web at http://apps.ecmwf.int/datasets/. And, the best tracks of tropical cyclones are collected from the International Best Track Archive for Climate Stewardship, which is available on the web at https://climatedataguide.ucar.edu/climate-data/ibtracs-tropical-cyclone-best-track-data.

Conflicts of Interest

The authors declare that they have no conflicts of interest.

Acknowledgments

The National Natural Science Funds of China supported this research through Grant nos. 41875039 and 41505014.

References

[1] S. Fujiwhara, "The natural tendency towards symmetry of motion and its application as a principle in meteorology," *Quarterly Journal of the Royal Meteorological Society*, vol. 47, pp. 287–292, 1921.

[2] S. Brand, "Interaction of binary tropical cyclones of the western North Pacific ocean," *Journal of Applied Meteorology*, vol. 9, no. 3, pp. 433–441, 1970.

[3] M. Lander and G. J. Holland, "On the interaction of tropical-cyclone-scale vortices. I: Observations," *Quarterly Journal of the Royal Meteorological Society*, vol. 119, no. 514, pp. 1347–1361, 1993.

[4] L. E. Carr III, M. A. Boothe, and R. L. Elsberry, "Observational evidence for alternate modes of track-altering binary tropical cyclone scenarios," *Monthly Weather Review*, vol. 125, no. 9, pp. 2094–2111, 1997.

[5] L. E. Carr III and R. L. Elsberry, "Objective diagnosis of binary tropical cyclone interactions for the western North Pacific basin," *Monthly Weather Review*, vol. 126, no. 6, pp. 1734–1740, 1998.

[6] M. A. Lander, "Specific tropical cyclone track types and unusual tropical cyclone motions associated with a reverse-oriented monsoon trough in the western North Pacific," *Weather and Forecasting*, vol. 11, no. 2, pp. 170–186, 1996.

[7] X. Xu, C. Lu, H. Xu, and L. Chen, "A possible mechanism responsible for exceptional rainfall over Taiwan from Typhoon Morakot," *Atmospheric Science Letters*, vol. 12, no. 3, pp. 294–299, 2011.

[8] X. Wu, J. Fei, X. Huang, X. Zhang, X. Cheng, and J. Ren, "A numerical study of the interaction between two simultaneous storms: Goni and Morakot in September 2009," *Advances in Atmospheric Sciences*, vol. 29, no. 3, pp. 561–574, 2012.

[9] H. Xu, X. Zhang, and X. Xu, "Impact of tropical storm Bopha on the intensity change of Super Typhoon Saomai in the 2006 typhoon season," *Advances in Meteorology*, vol. 2013, Article ID 487010, 13 pages, 2013.

[10] X. Luo, J. Fei, X. Huang, X. Cheng, and L. Liu, "Analysis of potential vorticity perspective on abnormal path of 1214 Typhoon Tembin," *Journal of the Meteorological Sciences*, vol. 34, pp. 119–127, 2014, in Chinese.

[11] Z. Zhu, N. Huang, and X. Wen, "Diagnostic analysis of interaction between binary typhoons Tembin and Bolaven," *Meteorological Science and Technology*, vol. 43, pp. 506–511, 2015, in Chinese.

[12] K. R. Knapp, M. C. Kruk, D. H. Levinson, H. J. Diamond, and C. J. Neumann, "The international best track archive for climate stewardship (IBTrACS)," *Bulletin of the American Meteorological Society*, vol. 91, no. 3, pp. 363–376, 2010.

[13] S. Fredrick, C. Davis, D. Gill, and S. Low-Nam, "Bogussing of tropical cyclones in WRF version 3.1," NCAR Technical Document P1.5, p. 6, 2009.

[14] S. Hong and J. J. Lim, "The WRF single–moment 6–class microphysics scheme (WSM6)," *Journal of the Korean Meteorological Society*, vol. 42, pp. 129–151, 2006.

[15] E. J. Mlawer, S. J. Taubman, P. D. Brown, M. J. Iacono, and S. A. Clough, "Radiative transfer for inhomogeneous atmospheres: RRTM, a validated correlated-k model for the longwave," *Journal of Geophysical Research: Atmospheres*, vol. 102, no. D14, pp. 16663–16682, 1997.

[16] J. Dudhia, "Numerical study of convection observed during the winter monsoon experiment using a mesoscale two-dimensional model," *Journal of the Atmospheric Sciences*, vol. 46, no. 20, pp. 3077–3107, 1989.

[17] M. Tewari and Coauthors, "Implementation and verification of the unified NOAH land surface model in the WRF model," in *Proceedings 20th Conference on Weather Analysis and Forecasting/16th Conference on Numerical Weather prediction*, pp. 11–15, American Meteor Society, Seattle, WA, USA, 2004.

[18] S.-Y. Hong, Y. Noh, and J. Dudhia, "A new vertical diffusion package with an explicit treatment of entrainment processes," *Monthly Weather Review*, vol. 134, no. 9, pp. 2318–2341, 2006.

[19] J. S. Kain, "The Kain-Fritsch convective parameterization: an update," *Journal of Applied Meteorology*, vol. 43, no. 1, pp. 170–181, 2004.

[20] C. E. Duchon, "Lanczos filtering in one and two dimensions," *Journal of Applied Meteorology*, vol. 18, no. 8, pp. 1016–1022, 1979.

[21] J. C. L. Chan and W. M. Gray, "Tropical cyclone movement and surrounding flow relationships," *Monthly Weather Review*, vol. 110, no. 10, pp. 1354–1374, 1982.

[22] J. C.-L. Chan, "An observational study of the physical processes responsible for tropical cyclone motion," *Journal of the Atmospheric Sciences*, vol. 41, no. 6, pp. 1036–1048, 1984.

[23] G. J. Holland, "Tropical cyclone motion. A comparison of theory and observation," *Journal of the Atmospheric Sciences*, vol. 41, no. 1, pp. 68–75, 1984.

[24] L. E. Carr III and R. L. Elsberry, "Observational evidence for predictions of tropical cyclone propagation relative to environmental steering," *Journal of the Atmospheric Sciences*, vol. 47, no. 4, pp. 542–546, 1990.

[25] C.-C. Wu and Y. Kurihara, "A numerical study of the feedback mechanisms of hurricane-environment interaction on hurricane movement from the potential vorticity perspective," *Journal of the Atmospheric Sciences*, vol. 53, no. 15, pp. 2264–2282, 1996.

[26] C.-C. Wu, T.-S. Huang, W.-P. Huang, and K.-H. Chou, "A new look at the binary interaction: potential vorticity diagnosis of the unusual southward movement of Tropical Storm Bopha (2000) and its interaction with Supertyphoon Saomai (2000)," *Monthly Weather Review*, vol. 131, no. 7, pp. 1289–1300, 2003.

[27] L. Wu and B. Wang, "A potential vorticity tendency diagnostic approach for tropical cyclone motion," *Monthly Weather Review*, vol. 128, no. 6, pp. 1899–1911, 2000.

[28] J. C. L. Chan, F. M. F. Ko, and Y. M. Lei, "Relationship between potential vorticity tendency and tropical cyclone motion," *Journal of the Atmospheric Sciences*, vol. 59, no. 8, pp. 1317–1336, 2002.

[29] M. Yuan, F. Ping, and G. Li, "Application of potential vorticity tendency in track recurvature study of typhoon Muifa," *Chinese Journal of Atmospheric Sciences*, vol. 42, pp. 281–291, 2018, in Chinese.

[30] P. J. Smith, "The kinetic energy budget over North America during a period of major cyclone development," *Tellus*, vol. 25, no. 5, pp. 411–423, 1973.

[31] Y. Sun, Z. Zhong, and Y. Wang, "Kinetic energy budget of Typhoon Yagi (2006) during its extratropical transition,"

Meteorology and Atmospheric Physics, vol. 118, no. 1-2, pp. 65–78, 2012.

[32] H. Abdel-Basset, M. A. A. Husin, and H. Hasanen, "Kinetic energy budget of a tropical cyclone," *Atmospheric and Climate Sciences*, vol. 5, pp. 394–407, 2015.

[33] Z. Cheng, L. Lin, G. Yang, and T. Sha, "Rapid intensification and associated large-scale circulation of super Typhoon Rammasun in 2014," *Journal of Applied Meterological Science*, vol. 3, pp. 318–326, 2017, in Chinese.

[34] W. M. Gray, "Global view of the origin of tropical disturbances and storms," *Monthly Weather Review*, vol. 96, no. 10, pp. 669–700, 1968.

[35] M. DeMaria, "The effect of vertical shear on tropical cyclone intensity change," *Journal of the Atmospheric Sciences*, vol. 53, no. 14, pp. 2076–2088, 1996.

[36] W. M. Frank and E. A. Ritchie, "Effects of vertical wind shear on the intensity and structure of numerically simulated hurricanes," *Monthly Weather Review*, vol. 129, no. 9, pp. 2249–2269, 2001.

[37] L. A. Paterson, B. N. Hanstrum, N. E. Davidson, and H. C. Weber, "Influence of environmental vertical wind shear on the intensity of hurricane-strength tropical cyclones in the Australian region," *Monthly Weather Review*, vol. 133, no. 12, pp. 3644–3660, 2005.

[38] Y. Wang, Y. Rao, Z.-M. Tan, and D. Schönemann, "A statistical analysis of the effects of vertical wind shear on tropical cyclone intensity change over the western North Pacific," *Monthly Weather Review*, vol. 143, no. 9, pp. 3434–3453, 2015.